Stability of the fragments and thermalization at peak center-of-mass energy

Aman D. Sood[1] and Sukhjit Kaur[2]

[1]*SUBATECH,*

Laboratoire de Physique Subatomique et des Technologies Associées

Université de Nantes - IN2P3/CNRS - EMN

4 rue Alfred Kastler, F-44072 Nantes, France.

[2]*Department of Physics, Panjab University, Chandigarh -160 014, India.*

June 15, 2011

Electronic address: amandsood@gmail.com

We simulate the central reactions of nearly symmetric, and asymmetric systems, for the energies at which the maximum production of IMFs occurs ($E_{c.m.}^{peak}$).This study is carried out by using hard EOS along with cugnon cross section and employing MSTB method for clusterization. We study the various properties of fragments. The stability

of fragments is checked through persistence coefficient and gain term. The information about the thermalization and stopping in heavy-ion collisions is obtained via relative momentum, anisotropy ratio, and rapidity distribution. We find that for a complete stopping of incoming nuclei very heavy systems are required. The mass dependence of various quantities (such as average and maximum central density, collision dynamics as well as the time zone for hot and dense nuclear matter) is also presented. In all cases (i.e., average and maximum central density, collision dynamics as well as the time zone for hot and dense nuclear matter) a power law dependence is obtained.

1 Introduction

The heavy-ion collisions at intermediate energies are excellent tool to study the nuclear matter at high density and temperature. At high excitation energies, the colliding nuclei compress each other as well as heat the matter [1–3]. This leads to the destruction of initial correlations, which in turn makes the matter homogeneous and one can have global stopping. The global stopping is defined as the randomization of one-body momentum space or memory loss of the incoming momentum. The degree of stopping, however, may vary drastically with incident energies, mass of colliding nuclei and colliding geometry. The degree of stopping has also been linked with the thermalization (equilibrium) in heavy-ion collisions. More the initial memory of nucleons is lost, better it is stopped.

The fragmentation of colliding nuclei into several pieces of different sizes is a complex phenomenon. This may be due to the interplay of correlations and fluctuations emerging in a collision. Several studies, in literature, have been made to check the fragmentation

pattern. Fragmentation pattern has been reported to depend on the size of the colliding nuclei, incident energy as well as impact parameter [1, 4–6]. Dhawan *et al.* [7] studied the degree of stopping reached in intermediate energy heavy-ion collisions. They found that degree of stopping decreases with increase in impact parameter as well as at very high energies. They suggested that the light charged particles (LCPs) ($2 \leq A \leq 4$), can be used as a barometer for studying the stopping in heavy-ion collisions. As lighter fragments mostly originate from midrapidity region whereas intermediate mass fragments (IMFs) originate from surface of colliding nuclei and can be viewed as remnants of the spectator matter. On the other hand, Sood and Puri [8] studied the thermalization achieved in heavy-ion collisions in terms of participant-spectator matter. They found that participant-spectator matter depends crucially on the collision dynamics as well as history of the nucleons and important changes in the momentum space occur due to the binary nucleon-nucleon collisions experienced during the high dense phase. The collisions push the colliding nucleons into midrapidity region responsible for the formation of participant matter. This ultimately leads to thermalization in heavy-ion collisions. Vermani *et al.* [8] used rapidity distribution of nucleons to characterize the stopping and thermalization of the nuclear matter. They found that nearly full stopping is achieved in heavier systems like ^{197}Au+^{197}Au whereas in lighter systems a larger fraction of particles is concentrated near target and projectile rapidities, resulting in a broad Gaussian shape. The lighter systems, therefore, exhibit larger transparency effect, i.e., less stopping. Puri *et al.* [9] studied the non-equilibrium effects and thermal properties of heavy-ion collisions. They found that the heavier masses are found to be equilibrated more than the lighter systems.

Recently, Sisan *et al.* [10] studied the emission of IMFs from central collisions of nearly

symmetric systems using a 4π-array set up, where they found that the multiplicity of IMFs shows a rise and fall with increase in the beam energy. They observed that $E_{c.m.}^{max}$ (the energy at which the maximum production of IMFs occurs) increases linearly with the system mass, whereas a power-law ($\propto A^{\tau}$) dependence was reported for peak multiplicity of IMFs with power factor $\tau = 0.7$. Though percolation calculations reported in that paper failed to explain the data, subsequent calculations using QMD model [11] successfully reproduced the data over entire mass. One is, therefore, interested to understands how nuclear dynamics behaves at this peak energy i.e. whether linear increase reported for the multiplicity of fragments remains valid for other observables or not. We here plan to investigate the degree of stopping reached and other related phenomena in heavy-ion reactions at peak center-of-mass energies. We also check system size dependence of average and maximum central density, collision dynamics as well as the time zone for hot and dense nuclear matter at peak center-of-mass energy.

This study is made within the framework of the quantum molecular dynamics model, which is described in detail in Refs. [1, 4, 11–18].

2 Results and Discussion

For the present study, we simulate the central reactions (b =0.0 fm) of ^{20}Ne+^{20}Ne, ^{40}Ar+^{45}Sc, ^{58}Ni+^{58}Ni, ^{86}Kr+^{93}Nb, ^{129}Xe+^{118}Sn, ^{86}Kr+^{197}Au and ^{197}Au+^{197}Au at the incident energies at which the maximal production of intermediate mass fragments (IMFs) occurs. These read approximately 24, 46, 69, 77, 96, 124, and 104 AMeV, respectively for the above mentioned systems [11]. Note that at lower incident energies phenomena like

fusion, fission and cluster decay are dominant [19]. Here we use hard (labeled as Hard) equation of state along with energy dependent Cugnon cross section (σ_{nn}^{free}) [15]. The reactions are followed till 200 fm/c. The phase-space is clusterized using minimum spanning tree method with binding energy check (MSTB). The MSTB method is an improved version of normal MST method [16]. Firstly, the simulated phase-space is analyzed with MST method and pre-clusters are sorted out. Each of the pre-clusters is then subjected to binding energy check [11, 16]:

$$\zeta_i = \frac{1}{N^f}\sum_{i=1}^{N^f}[\frac{(\mathbf{p}_i - \mathbf{P}_{N^f}^{c.m.})^2}{2m_i} + \frac{1}{2}\sum_{j\neq i}^{N^f} V_{ij}(\mathbf{r}_i, \mathbf{r}_j)] < E_{bind}. \quad (1)$$

We take E_{bind} = -4.0 MeV if $N^f \geq 3$ and E_{bind} = 0.0 otherwise. Here N^f is the number of nucleons in a fragment and $\mathbf{P}_{N^f}^{c.m.}$ is center-of-mass momentum of the fragment. This is known as Minimum Spanning Tree method with Binding energy check (MSTB) [11, 16]. Note that nucleons belong to a fragment if inequality (1) is satisfied. The fragments formed with the MSTB method are more reliable and stable at early stages of the reactions.

One of the important aspects in fragmentation is the stability of fragments as well as surrounding nucleons of a fragment. The change in the nucleon content of fragments between two successive time steps can be quantified with the help of persistence coefficient [17, 18].

Let the number of pairs of nucleons in cluster C at time t is $\chi_C(t)$=0.5$*N_C(N_C$-1). At the time Δt later, it is possible that some of the nucleons belonging to cluster C have left the cluster and are the part of another cluster or are set free or others may have entered the cluster. Now, let N_{C_D} be the number of nucleons that have been in the cluster C at

time t and are at $t + \Delta t$ in cluster D. We define

$$\Phi_C(t + \Delta t) = \sum_D 0.5 * N_{C_D}(N_{C_D} - 1). \tag{2}$$

Here the sum runs over all fragments D present at time $t + \Delta t$.

The persistence coefficient of cluster C can be defined as [17, 18]:

$$P_C(t + \frac{\Delta t}{2}) = \Phi_C(t + \Delta t)/\chi_C(t). \tag{3}$$

The persistence coefficient averaged over an ensemble of fragments is defined as:

$$\langle P(t + \frac{\Delta t}{2})\rangle = \frac{1}{N_{f_t}} \sum_C P_C(t + \frac{\Delta t}{2}), \tag{4}$$

where N_{f_t} is the number of fragments present at time t in a single simulation. The quantity is then averaged over a large number of QMD simulations. The stability of a fragment between two consecutive time steps can be measured through persistence coefficient. If fragment does not emit a nucleon between two time steps, the persistence coefficient is one. On the other hand, if fragment disintegrates completely, the persistence coefficient will be zero. If we remove one nucleon from a fragment C, the persistence coefficient is $\mathrm{P}_C(t + \Delta t/2) = (\mathrm{N}_C\text{-}2)/\mathrm{N}_C$ i.e., 0.333 for $\mathrm{N}_C = 3$ and 0.8 for $\mathrm{N}_C = 10$. For example for mass 10, when one nucleon is emitted we have two entities at later time step consisting of free nucleon and fragment with mass 9. The $\mathrm{P}_C(t + \Delta t/2)$ is the contribution from all such entities existing at later times. It, then, measures the tendency of the members of given cluster to remain together. In fig. 1, we display the persistence coefficient for various fragments i.e., light charged particles (LCPs) ($2 \leq \mathrm{A} \leq 4$), intermediate mass fragments (IMFs) ($5 \leq \mathrm{A} \leq 44$) as well as heavy mass fragments (HMFs) ($10 \leq \mathrm{A} \leq 44$). The various lines have been defined in the caption. It is clear from fig. that the saturation

value of persistence coefficient is slightly higher in case of LCPs as compared to heavier fragments. One can conclude that the final fragments are formed after 130 fm/c when this coefficient is 0.8. Before that time there is a strong exchange of nucleons between the fragments. The number of medium and intermediate size fragments increases because the largest fragment falls finally into this mass bracket. The persistent coefficient reaches its asymptotic value later due to the interaction between fragments as well as between fragments and free nucleons. Due to this interaction nucleons are sometimes absorbed or emitted from the fragments. This process changes the details but not the general structure of the fragmentation pattern.

The persistence coefficient tells about the stability of different fragments between two successive time steps. But it does not provide any information whether a fragment has swallowed some nucleons or not. To check this, we use a quantity called "Gain" [18]. The Gain represents the percentage of nucleons that a fragment has swallowed between two consecutive time steps. Let N_{α}^{f} be the number of nucleons belong to a fragment α at time t. Let $\mathrm{N}_{\alpha\beta}^{f}$ be the number of nucleons which were in cluster α at time t and are in cluster β at time $t + \Delta t$. The Gain is defined as:

$$Gain(t + \Delta t/2) = \sum_{\alpha} \eta \times \frac{\sum_{\beta}(N_{\beta}^{f} - N_{\alpha\beta}^{f})}{N_{\alpha}^{f}}; \tag{5}$$

$\eta = 0.0$, 0.5, and 1.0 if $\mathrm{N}_{\alpha\beta}^{f} < 0.5\ \mathrm{N}_{\beta}^{f}$, $\mathrm{N}_{\alpha\beta}^{f} = 0.5\ \mathrm{N}_{\beta}^{f}$ and $\mathrm{N}_{\alpha\beta}^{f} > 0.5\ \mathrm{N}_{\beta}^{f}$, respectively. Naturally, a true Gain for a fragment α is only if its nucleons constitute at least half of the mass of new fragment β. The Gain term will tell us whether the interactions among fragments have ceased to exist or not.

In fig. 2, we display the gain term for LCPs, HMFs, and IMFs. As discussed earlier,

the value of persistence coefficient is slightly higher in case of LCPs. Therefore, gain term will be smaller for LCPs as shown in fig. 2. As evident from fig., in case of heavier systems the gain term has higher value because of the large nucleon-nucleon interactions.

The quantities which are closely related to the degree of thermalization are relative momentum $\langle K_R \rangle$ and anisotropy ratio $\langle R_a \rangle$. The average relative momentum of two colliding fermi spheres is defined as [3, 9, 20]:

$$\langle K_R \rangle = \langle |P_P(\mathbf{r}, t) - P_T(\mathbf{r}, t)|/\hbar \rangle, \tag{6}$$

where

$$P_k(\mathbf{r}, t) = \frac{\sum_{j=1}^{A_k} P_j(t)\rho_j(\mathbf{r}, t)}{\rho_k(\mathbf{r}, t)}. \tag{7}$$

Here P_j and ρ_j are the momentum and density experienced by j^{th} particle and k stands for either target or projectile and $\mathbf{r}$ refers to a space point in central sphere of 2 fm radius to which all calculations are made. The $\langle K_R \rangle$ is an indicator of local equilibrium because it depends on the local position r .

The second quantity is anisotropy ratio which is defined as [3, 7, 9, 20]:

$$\langle R_a \rangle = \frac{\sqrt{\langle p_x^2 \rangle} + \sqrt{\langle p_y^2 \rangle}}{2\sqrt{\langle p_z^2 \rangle}}. \tag{8}$$

The anisotropy ratio $\langle R_a \rangle$ is an indicator of global equilibrium of the system because it represents the equilibrium of the whole system and does not depend upon the local positions. The full global equilibrium averaged over large number of events will correspond to $\langle R_a \rangle = 1$.

In figs. 3a and 3b, we display, respectively, $\langle K_R \rangle$ and $\langle R_a \rangle$ ratio as a function of time for different system masses. The initial value of relative momentum increases whereas of

the anisotropy ratio decreases with mass of the system since $E_{c.m.}^{peak}$ increases with increase in the system mass. It is interesting to see that the relative momentum is large at the start of the reaction, and finally at the end of the reaction, the value of $\langle K_R \rangle$ is nearly zero. This means that at the end of the reaction, the local equilibrium is nearly reached. However, the saturation time is nearly the same throughout the mass range. It is clear from the fig. 3b anisotropy ratio changes to a greater extent during the high density phase. Once the high density phase is over, no more changes occur in thermalization. Interestingly, the heavier nuclei are able to equilibrate more than the lighter nuclei. This is because of the fact that the number of collisions per nucleon for the ^{197}Au+^{197}Au reaction is larger than for the ^{58}Ni+^{58}Ni reaction.

The rapidity distribution is also assumed to give information about the degree of thermalization achieved in heavy-ion reactions. The rapidity distribution of i^{th} particle is defined as [7]:

$$Y(i) = \frac{1}{2} \ln \frac{\mathbf{E}(i) + \mathbf{p}_z(i)}{\mathbf{E}(i) - \mathbf{p}_z(i)}, \tag{9}$$

Here $\mathbf{E}(i)$ and $\mathbf{p}_z(i)$ are, respectively, the total energy and longitudinal momentum of i^{th} particle. Naturally, for a complete equilibrium a single Gaussian shape peak is expected. In fig. 4, we display the rapidity distribution of free-nucleons, LCPs, HMFs as well as IMFs. Rapidity distribution of all types of fragments indicate that heavier systems are better thermalized as compared to lighter ones. For lighter nuclei, we get relatively flat distribution. The effect is more pronounced for different kinds of fragments as compared to free-nucleons.

In fig. 5, we display the system size dependence of the maximal value of average density $\langle \rho^{avg} \rangle$ (solid circles) and maximum density $\langle \rho^{max} \rangle$ (solid stars). Lines represent

the power law fitting ($\propto$ A$^{\tau}$). The maximal values of $\langle\rho^{avg}\rangle$ and $\langle\rho^{max}\rangle$ follow a power law ($\propto$ A$^{\tau}$) with τ being 0.08$\pm$0.02 for the average density $\langle\rho^{avg}\rangle$ and 0.034$\pm$0.008 for maximum density $\langle\rho^{max}\rangle$ i.e., a slight increase in density occurs with increase in the size of the system. This is because, E$^{peak}_{c.m.}$ increases with the size of the system.

In fig. 6, we display the time of maximal collision rate (open stars) and average density $< \rho_{avg} >^{max}$ (solid circles) as a function of the total mass of the system. Interestingly, both quantities show a nearly mass independent behavior which shows that E$^{peak}_{c.m.}$ increases with the mass of the system in such a way that maximal collision rate and maximal density is achieved at the same time throughout the mass range. The power factor being equal to -0.017$\pm$0.038 for maximal time of collision rate and 0.015$\pm$0.07 for maximal time of average density.

Apart from the maximal quantities, another interesting quantity is the dense zone at the peak energy. In fig. 7, we display the time interval for which $\rho_{avg} \geq \rho_o$ (solid circles) and $\rho_{avg} \geq \rho_o/2$ (open stars). Again both quantities follow a power law behavior with τ = 0.15$\pm$0.05 and τ= -0.04$\pm$0.06, respectively, for $\rho_{avg} \geq \rho_o$ and $\rho_{avg} \geq \rho_o/2$. This indicates that the time duration for which ρ_{avg} is greater than the normal nuclear matter density increases with the mass of the system.

The system size dependence of the (allowed) nucleon-nucleon collisions (solid squares) is displayed in fig. 8. The results are displayed at 200 fm/c where the matter is diluted and well separated. The nucleon-nucleon collisions increase with the system size. This enhancement can be parametrized with a power law proportional to A$^{\tau}$ with τ = 1.28$\pm$0.054. At fixed incident energy nucleon-nucleon collisions should scale as A. This has been tested by Sood and Puri [21]. Here power factor is greater than one since with

increase in mass of the system $E_{c.m.}^{peak}$ also increases.

3 Summary

In the present study, we have simulated the central reactions of nearly symmetric, and asymmetric systems, for the energies at which the maximum production of IMFs occurs ($E_{c.m.}^{peak}$), using QMD model. This study is carried out by using hard EOS along with cugnon cross section and employing MSTB method for clusterization. We have studied the various properties of fragments. The stability of fragments is checked through persistence coefficient and gain term. The information about the thermalization and stopping in heavy-ion collisions is obtained via relative momentum, anisotropy ratio, and rapidity distribution. We found that for a complete stopping of incoming nuclei very heavy systems are required. The mass dependence of various quantities (such as average and maximum central density, collision dynamics as well as the time zone for hot and dense nuclear matter) is also presented. In all cases (i.e., average and maximum central density, collision dynamics as well as the time zone for hot and dense nuclear matter) a power law dependence is obtained.

References

[1] P. B. Gossiaux and J. Aichelin, Phys. Rev. C **56**, 2109 (1997).

[2] R. K. Puri *et al.*, Nucl. Phys. A **575**, 733 (1994); Y. K. Vermani and R. K. Puri, Nucl. Phys. A **847**, 243 2010.

[3] D. T. Khoa *et al.*, Nucl. Phys. A **548**, 102 (1992).

[4] J. Aichelin, Phys. Rep. **202**, 233 (1991).

[5] M. B. Tsang *et al.*, Phys. Rev. Lett. **71**, 1502 (1993).

[6] C. Williams *et al.*, Phys. Rev. C **55**, R2132 (1997).

[7] J. K. Dhawan *et al.*, Phys. Rev. C **74**, 057901 (2006).

[8] A. D. Sood *et al.*, Int. J. Mod. Phys. E **15**, 899 (2006); Y. K. Vermani *et al.*, Phys. Rev. C **79**, 064613 (2009).

[9] R. K. Puri *et al.*, J. Phys. G: Nucl. Part. Phys. **20**, 1817 (1994).

[10] D. Sisan *et al.*, Phys. Rev. C **63**, 027602 (2001).

[11] Y. K. Vermani *et al.*, J. Phys. G: Nucl. Part. Phys. **36**, 105103 (2009); S. Kaur and A. D. Sood, Phys. Rev. C **82**, 054611 (2010).

[12] C. Hartnack *et al.*, Eur. Phys. J A **1**, 151 (1998); S. W. Huang *et al.*, Phys. Lett. B **298**, 41 (1993); Y. K. Vermani and R. K. Puri, Europhys. Lett. **85**, 62001 (2009); Y. K. Vermani *et al.*, J. Phys. G: Nucl. Part. Phys. **37**, 015105 (2010); S. Kumar *et al.*, Phys. Rev. C **78**, 064602 (2008).

[13] S. Kumar *et al.*, Phys. Rev. C **58**, 3494 (1998); E. Lehmann *et al.*, Z. Phys. A **355**, 55 (1996); A. D. Sood *et al.*, Phys. Rev. C **79**, 064618 (2009); S. Kumar *et al.*, Phys. Rev. C **81**, 014611 (2010); *ibid* **81**, 014601 (2010); E. Lehmann *et al.*, Prog. Part. Nucl. Phys. **30**, 219 (1993); E. Lehmann *et al.*, Phys. Rev. C **51**, 2113 (1995).

[14] J. Singh *et al.*, Phys. Rev. C **62**, 044617 (2000); G. Batko *et al.*, J. Phys. G: Nucl. Part. Phys. **20**, 461 (1994); S. W. Huang *et al.*, Prog. Part. Nucl. Phys. **30**, 105 (1993); C. Fuchs *et al.*, J. Phys. G: Nucl. Part. Phys. **22**, 131 (1996); A. D. Sood *et al.*, Phys. Lett. B **594**, 260 (2004); *ibid* Phys. Rev C **73**, 067602 (2006); S. Gautam *et al.*, J Phys. G: Nucl. Part. Phys. **37**, 085102 (2010).

[15] S. Kumar *et al.*, Phys. Rev. C **58**, 1618 (1998); Y. K. Vermani *et al.*, Phys. Rev. C **79**, 064613 (2009); R. Chugh and R. K. Puri, Phys. Rev. C **82**, 014603 (2010).

[16] J. Singh *et al.*, J. Phys. G: Nucl. Part. Phys. **27**, 2091 (2001); S. Kumar *et al.*, Phys. Rev. C **58**, 2858 (1998).

[17] R. K. Puri and J. Aichelin, J. Comp. Phys. **162**, 245 (2000); R. K. Puri *et al.*, Phys. Rev. C **54**, R28 (1996); P. B. Gossiaux *et al.*, Nucl. Phys. A **619**, 379 (1997).

[18] R. K. Puri *et al.*, Pram. J. Phys. **59**, 19 (2002).

[19] I. Dutt *et al.*, Phys. Rev. C **81**, 047601 (2010); *ibid* **81**, 044615 (2010); *ibid* **81**, 064609 (2010); *ibid* **81**, 064608 (2010); R. Arora *et al.*, Eur. Phys. J A **8**, 103 (2000); R. K. Puri *et al.*, Phys. Rev. C **43**, 315 (1991); *ibid* **45**, 1837 (1992); *ibid* J. Phys. G: Nucl.Part Phys. **18**, 903 (1992); *ibid* Eur. Phys. J A **3**, 277 (1998); *ibid* Eur. Phys. J A **23**, 429 (2005).

[20] D. T. Khoa *et al.*, Nucl. Phys. A **529**, 363 (1991).

[21] A. D. Sood *et al.*, Phys. Rev. C **70**, 034611 (2004).

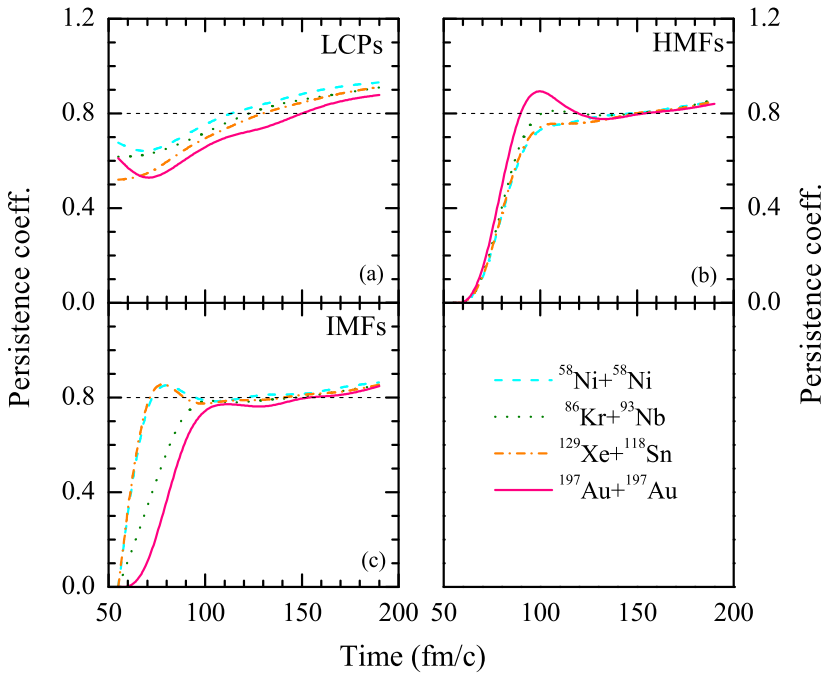

Figure 1: The persistence coefficient as a function of time for LCPs, HMFs, and IMFs. Dashed, dotted, dash-dotted and solid lines are for ^{58}Ni+^{58}Ni, ^{86}Kr+^{93}Nb, ^{129}Xe+^{118}Sn and ^{197}Au+^{197}Au, respectively.

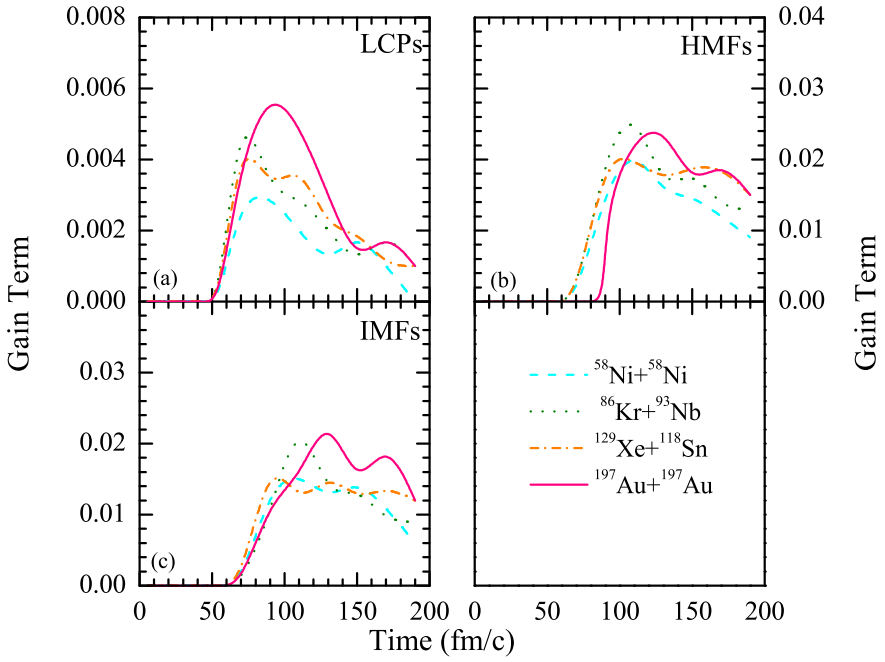

Figure 2: The Gain term as a function of time for LCPs, HMFs, and IMFs. Lines have same meaning as in fig. 1.

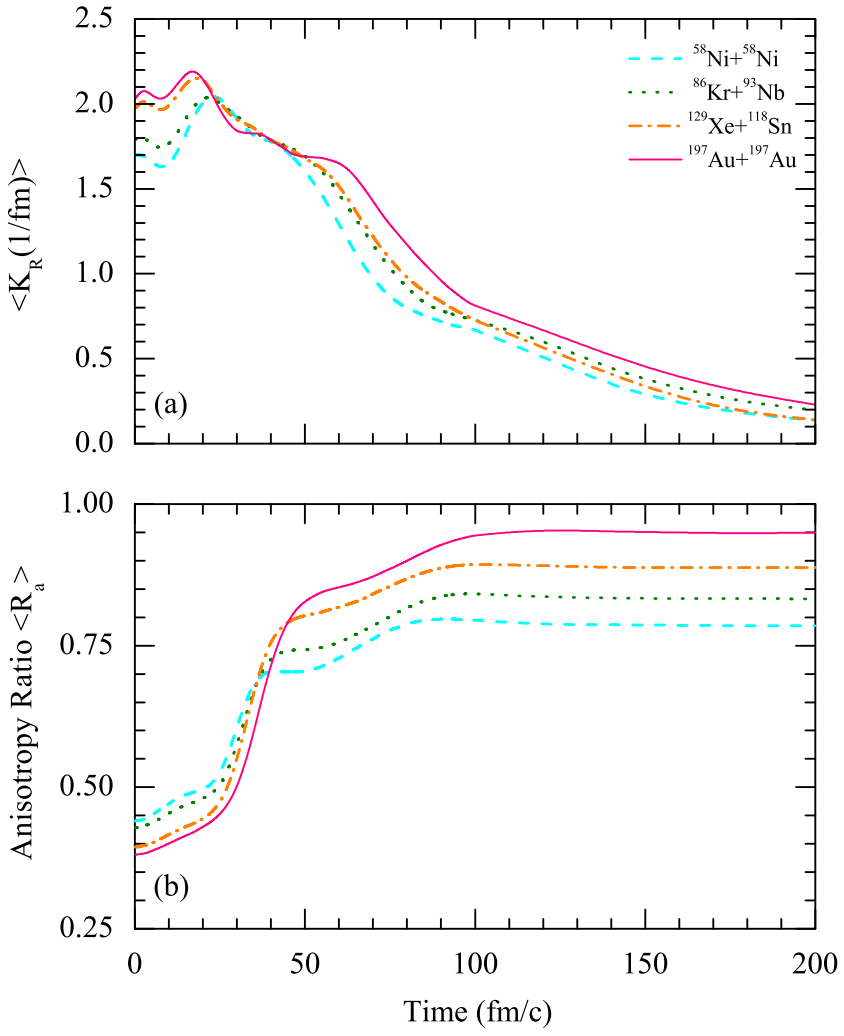

Figure 3: The time evolution of (a) relative momentum and (b) anisotropy ratio. Lines have same meaning as in fig. 1.

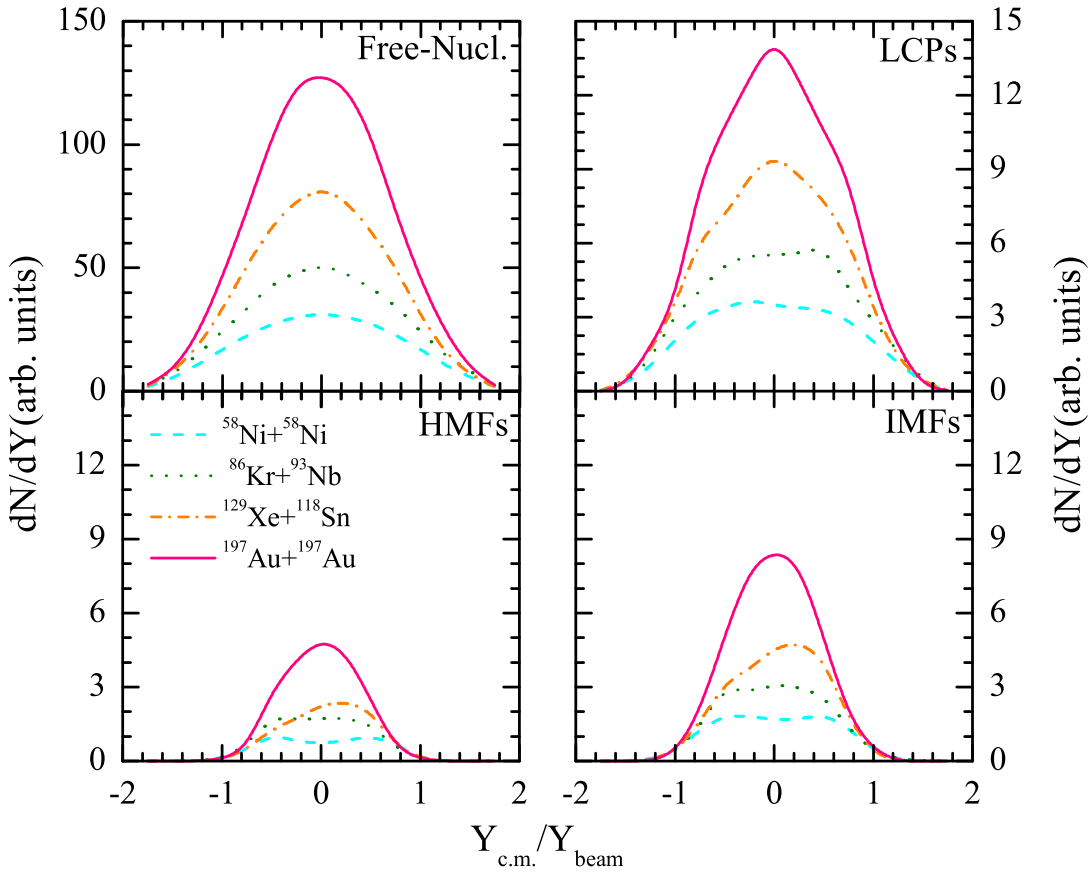

Figure 4: The rapidity distribution, dN/dY, as a function of reduced rapidity, $Y_{c.m.}/Y_{beam}$. Lines have same meaning as in fig. 1.

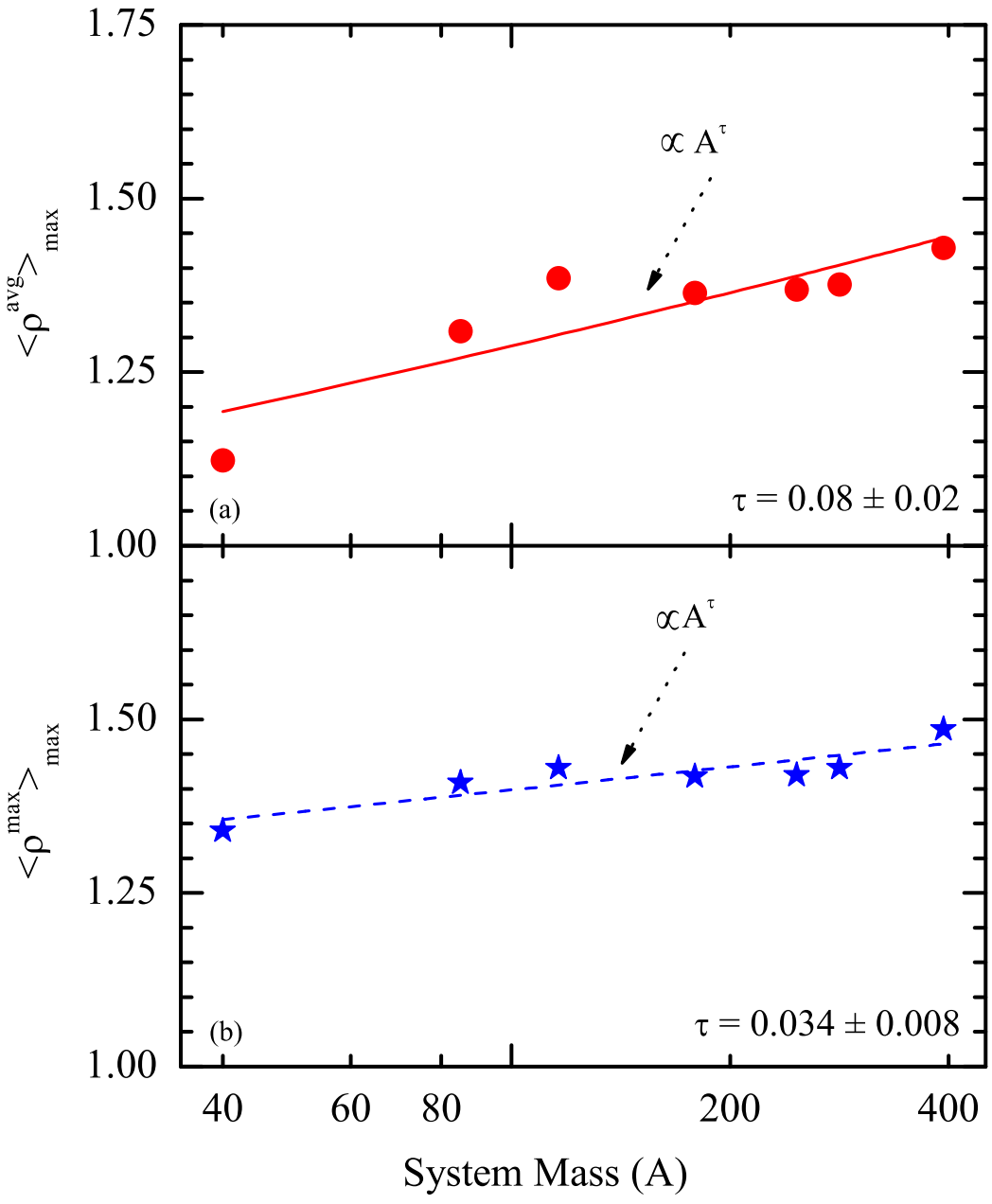

Figure 5: The maximal value of the average density $\langle \rho^{avg} \rangle_{max}$ (upper part) and maximum density $\langle \rho^{max} \rangle_{max}$ (lower part) as a function of the composite mass of the system. The solid lines are the fits to the calculated results using A^{τ} obtained with χ^2 minimization. The average is done over all space points on a sphere of 2 fm radius at center-of-mass.

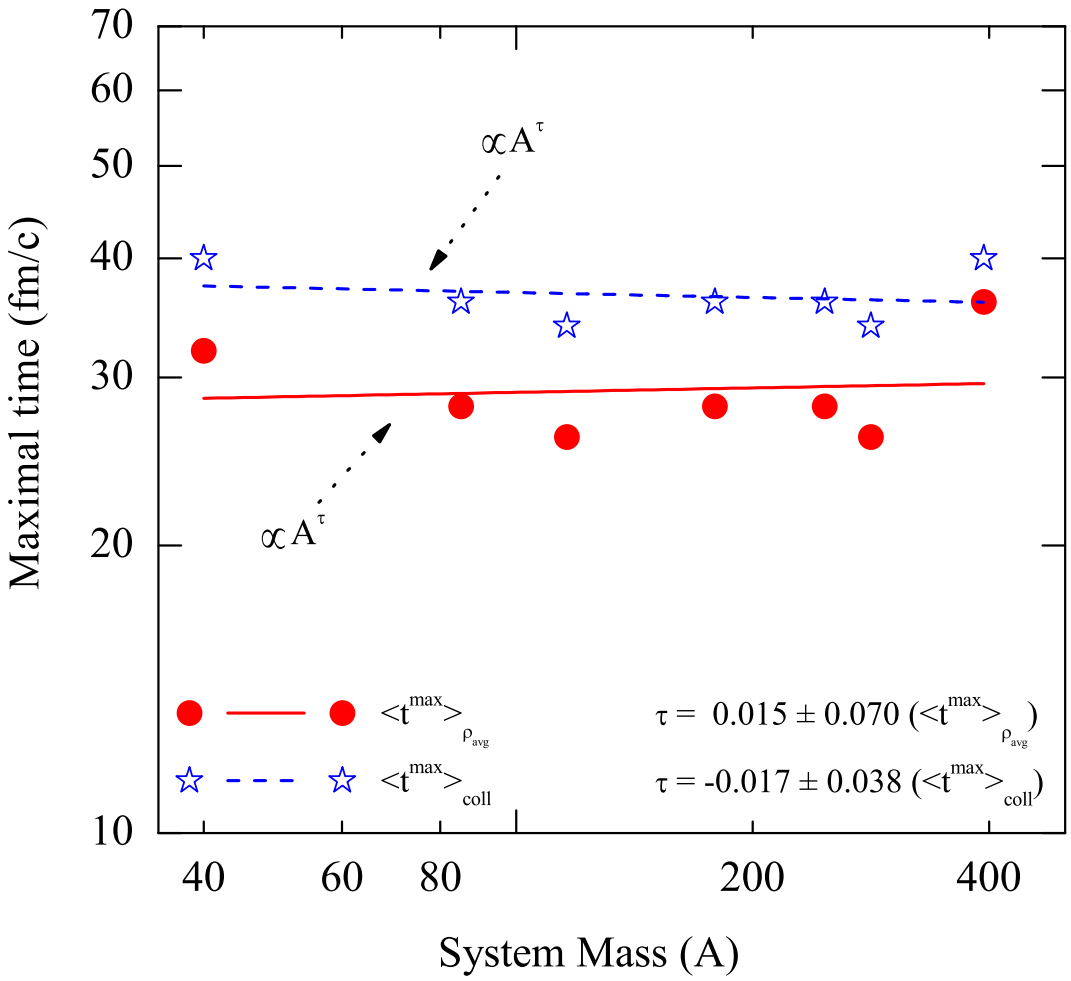

Figure 6: The time of maximal value of collision rate (open stars) and average density (solid circles) as a function of composite mass of the system. The dashed and solid lines represent the χ^2 fits with power law A^τ.

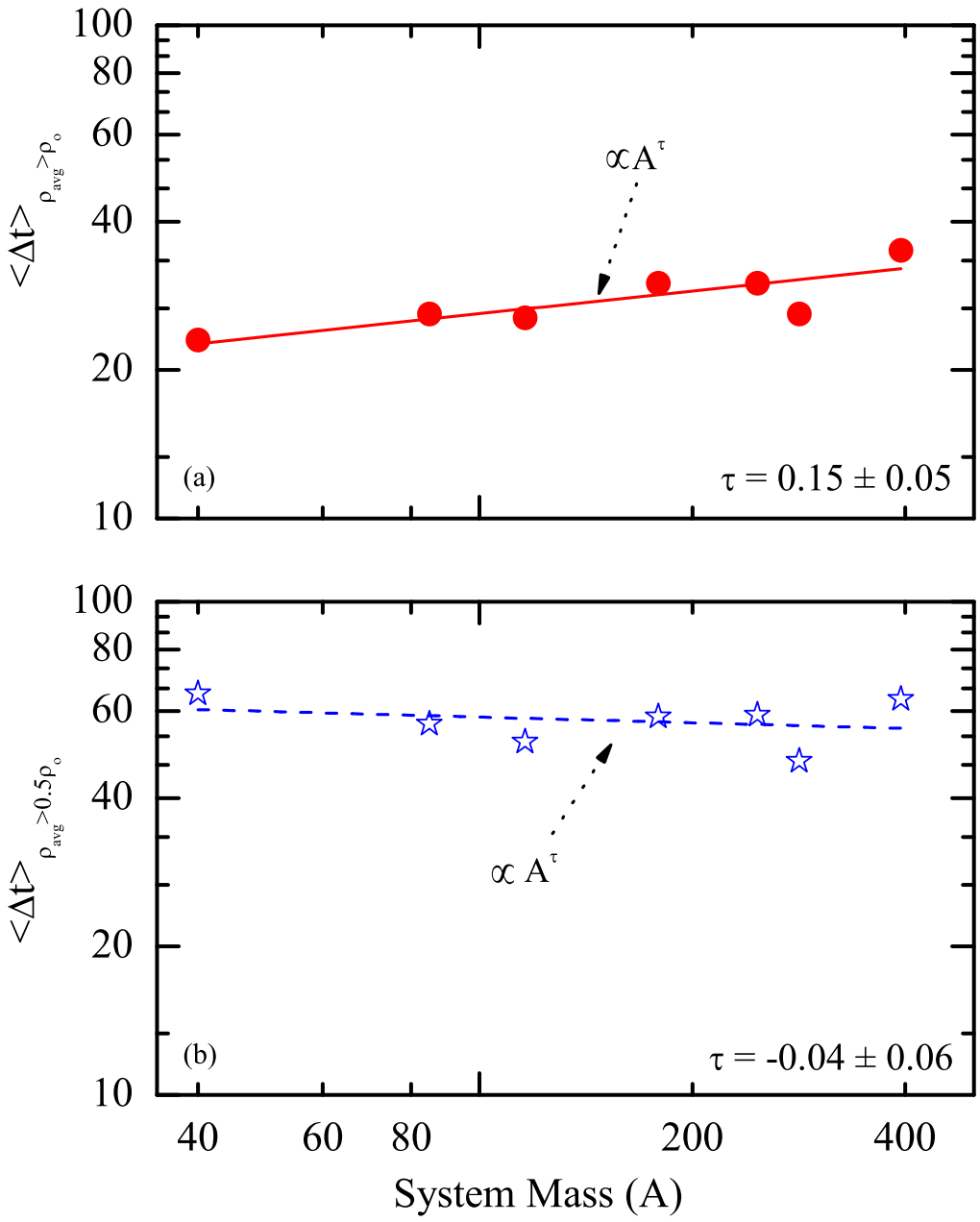

Figure 7: The time zone for $\rho_{avg} \geq \rho_o$ (upper part) and for$\rho_{max} \geq \rho_o$ (lower part) as a function of composite mass of the system. The solid lines represent the the χ^2 fits with power law A^{τ}.

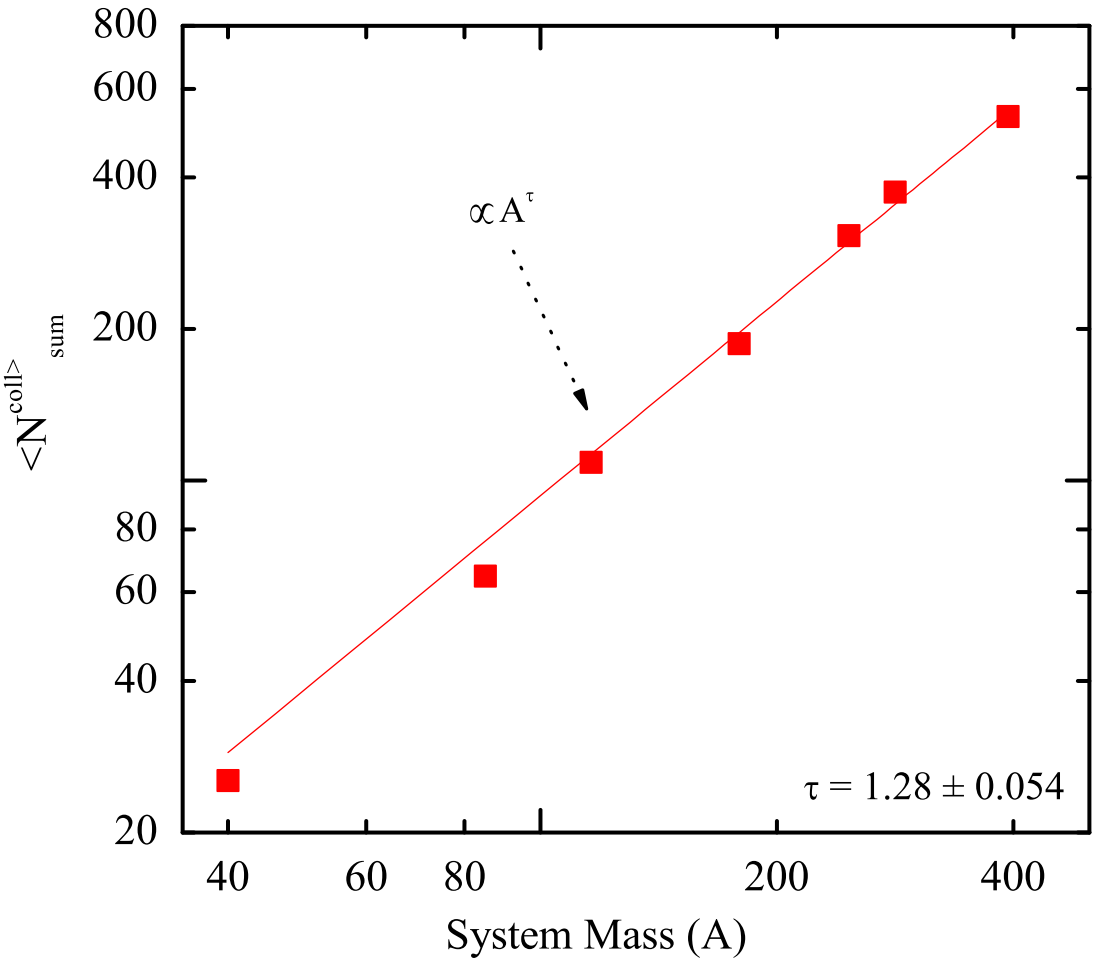

Figure 8: The total number of allowed collisions versus composite mass of the system. The solid line represents the χ^2 fits with power law A^{τ}.